Tunable p- and n-Type Tellurium-free Mg_3Bi_2 Thermoelectric Thin Films by Thermal Co-Evaporation

Joost W.C. Reinders,[a] Cristina Roldán-Carmona,[a] Henk J. Bolink,[a]* and Francisco Palazon[b]*

[a] Instituto de Ciencia Molecular, Universidad de Valencia, 46980 Paterna, Spain

[b] Departamento de Ingeniería Química y Ambiental, Universidad Politécnica de Cartagena, 30202 Cartagena, Spain

Keywords: Thermoelectrics, Room-temperature, Thin Film, Co-evaporation, Mg_3Bi_2

ABSTRACT: Mg_3Bi_2 has recently emerged as a promising environmentally-friendly alternative to bismuth tellurides for near-room-temperature thermoelectrics. Here, we report on the fabrication of Mg_3Bi_2 thin films under Mg-rich and Mg-poor conditions via vacuum thermal co-evaporation. We demonstrate that under Mg-deficient conditions, thin films show a p-type conduction behavior with a maximum power factor exceeding 300 μW/(m·K^2) and a thermoelectric figure of merit *ZT* of 0.11 at 200 °C. Increasing the amount of Mg enables the formation of Mg-rich Mg_3Bi_2 thin films with n-type conduction. These films exhibit a maximum power factor and *ZT* at lower temperatures around 130-140 °C. Moreover, the maximum *ZT* is increased to 0.19 owing to the ultra-low thermal conductivity of the n-type Mg_3Bi_2.

INTRODUCTION

Thermoelectrics (TE) represents one of the main potential sources of renewable energy for the near future. Indeed, "waste" heat is produced ubiquitously from industrial processes to the human body. Thus, taking advantage of this energy source to produce usable electrical power is of great interest. Thermoelectric generators (TEGs) make use of p- and n-type semiconductors that translate a temperature difference into an electrical potential difference (voltage) through the well-known Seebeck effect. A TEG works by combining several "legs" of n- and p-type TE materials placed thermally in parallel between a hot and cold source and electrically in series.[1] In order to maximize the potential power output of a TEG, the TE materials must maximize their dimensionless figure of merit *ZT* which is defined as follows:

$$ZT = (\sigma S^2/\kappa)T$$

where σ, S, κ, and T are the electrical conductivity, the Seebeck coefficient, the thermal conductivity, and the absolute temperature, respectively.

One of the proposed applications of TE is the self-powering of small, lightweight and flexible electronic devices such as wearable sensors.[2,3] However, in order to be able to implement TEGs in such applications, the TE materials must be processed as thin films, without toxic elements and with relevant *ZT* values around room temperature (RT).[4–6] Most TE materials reported so far fail to meet these criteria as they: (i) use scarce and toxic elements such as tellurium and/or toxic heavy metals, and/or (ii) have maximum *ZT* values achieved at high temperatures (*e.g.*, 783 K for SnSe which holds the current record value of *ZT*=3.1),[7] and/or (iii) are synthesized in the form of bulk millimetric crystals or pellets limiting their integration into miniaturized thin film technologies.[8]

The field of (flexible) thin film thermoelectric materials for RT applications is not new. For example, *Ao et al.* demonstrated the fabrication of a flexible Sb_2Te_3/Bi_2Te_3 thin film TEG with a power density of 1.42 mW cm^{-2} at a temperature difference of 60 K[9], while *Wei et al.* reached a power density of >280 μW cm^{-2} at a temperature difference of 20 K with a TEG composed of $(Sb_2Te_3)(Te)_{1.5}$ and Bi_2Te_3.[10] Although showing promising results, these materials are based on scarce and toxic tellurium which limit their application in wearable self-powered devices.

Mg_3Bi_2 and related Zintl materials, such as Mg_3Sb_2, have recently been reported as promising TE candidates for near RT applications.[11–13] Initial studies show that their TE properties are comparable to that of bismuth tellurides when operated near RT.[14–16] Mg_3Bi_2 has been reported as a p-type semimetal, whose electrical conduction is governed by the presence of Mg vacancies.[11] As a result, increasing the Mg content has been shown to lead to an important change in electrical properties, with Mg-rich compositions showing n-type behavior. The highest *ZT* that was recorded for undoped p-type Mg_3Bi_2 is around 0.1 across a temperature range of 300 – 825 K.[17] Other reports[18] have achieved a *ZT* of ~0.25 with a composition labelled as $Mg_{3+\delta}Bi_2$; however this composition also contains some tellurium as the full composition is $Mg_{3+\delta}Bi_{1.99}Te_{0.01}$:$Mn_{0.01}$. Addition of extrinsic dopants has proven to be a useful way to increase the thermoelectric properties of Mg_3Bi_2 and related compounds.[19,20] The (partial) substitution of Bi with Sb and doping with S, Se, or Te led to an increase of the charge carrier concentration as well as to lower thermal conductivities (due to phonon scattering) providing a promising way of tuning the TE properties.[21–23] However, additional extrinsic dopants add complexity to the process and, in case of elements such as tellurium, raise concerns on toxicity and scarcity. Other efforts to improve the thermoelectric properties of Mg_3Bi_2-based compounds include tuning the ratio of Mg and Bi.[24–26] Increasing the Mg content in

$Mg_{3+x}Sb_{1.5}Bi_{0.49}Te_{0.01}$ beyond the nominal amount compensates for Mg vacancies in the crystal structure and allows for a significantly higher charge carrier concentration.[24]

A well-established preparation method of this class of TE materials involves the mechanical alloying of the constituents until the desired composition is formed, after which the resulting powder is turned into a mm-sized pellet using hot pressing.[19,21,22] These pellets have only recently been successfully introduced in a TEG module by *Ying et. al.*, reaching a conversion efficiency of ~7.0% at a temperature difference of around 250 K.[27] Despite the promising developments and relatively high conversion efficiency for near RT applications, these bulk thermoelectric modules lack the flexibility and scalability for wearable applications.

Recent work by *Sadowski et al.* has demonstrated the fabrication of Mg_3Bi_2 thin films via sputtering, enabling their use in the field of flexible wearables and related applications.[28] The authors reported a maximum power factor (*PF*) of 200 $\mu W \cdot m^{-1} \cdot K^{-1}$ near room temperature on p-type Mg_3Bi_2 thin films grown at a substrate temperature of 200 °C. However, the thermal conductivity is not measured and hence no *ZT* value can be derived from this work. In another work *Fang et al.* demonstrated that varying the substrate temperature during the sputtering process induces a phase transition in the Mg_3Bi_2, with a maximum *PF* of 110 $\mu W \cdot m^{-1} \cdot K^{-1}$ at 393 K.[29] *Tani et al.* explored the formation of Mg_3Bi_2 thin films by post-annealing Mg/Bi bilayers prepared by magnetron sputtering.[30] Although the authors obtained a homogeneous composition, the *PF* of their Mg_3Bi_2 film was limited to 89 $\mu W \cdot m^{-1} \cdot K^{-1}$ at 565 K. The existing literature on Mg_3Bi_2 thin films lack thermal conductivity measurements, limiting the understanding of Mg_3Bi_2 and hinders the assessment of its potential as thermoelectric material in TEGs. These studies also mention that thermal vacuum deposition of Mg_3Bi_2 thin films is challenging due to the high vapor pressure of Mg and that therefore sputtering is the preferred deposition method for these alloys.[28] However, already in 1979 *Long et. al.* reported on the thermal co-evaporation of Mg and Bi and the formation of a two-component alloy in which the compositional variations were below 0.5%.[31] The reliability of thermal evaporation of Mg is supported by other studies focusing on the co-evaporation of Mg and B to form MgB thin films.[32,33] These considerations make thermal co-evaporation of said constituents a promising technique to fabricate Mg_xBi_y thin films.

In this work we have deposited Mg_3Bi_2 thin films (thicknesses around 350 nm) without extrinsic dopants (such as scarce and toxic Te) by thermal vacuum co-deposition of elemental Mg and Bi. Morphological, elemental, and structural characterization is carried out by Scanning Electron Microscopy (SEM), Energy-Dispersive X-ray Spectroscopy (EDS), and X-Ray Diffraction (XRD) to prove the successful formation of these materials as thin films. Furthermore, we investigate the effect of the material stoichiometry on the thermoelectric properties. We find that depending on the stoichiometry both p- or n-type materials can be obtained with *ZT* values in excess of 0.1 near room temperature. This represents, to the best of our knowledge, the highest reported *ZT* on tellurium-free Mg_3Bi_2 materials and the first full thermoelectric characterization of these alloys in the form of thin films. Compared to previous results reported on films deposited by magnetron sputtering,[28] it is important to highlight that our method based on thermal evaporation does not use substrate heating during deposition, allows for tunable p- and n-type films, and yields higher power factors up to 300 $\mu W \cdot m \cdot K^{-1}$ making it a promising approach for flexible miniaturized TEGs.

In short, Mg_3Bi_2 thin films are prepared by thermal co-evaporation of Mg and Bi in a vacuum chamber (see Supporting Information for the experimental details). Typically, a film of approximately 350 nm is grown in about 35 min. The evaporation rate of Bi is fixed to 1.00 Å/s (source temperature = 560 °C) while the evaporation rate of Mg is set either to 0.98 Å/s (source temperature = 330 °C) or 1.11 Å/s (source temperature = 340 °C) to prepare Mg-poor or Mg-rich compositions, respectively. Elemental analysis by EDS yields a composition of $Mg_{3.2}Bi_2$ and $Mg_{3.5}Bi_2$ in these conditions, respectively (see Figure S1). This confirms that the increased evaporation rate leads to an increase of Mg incorporated in the thin film. The film grown with an Mg evaporation rate of 0.98 Å/s shows a p-type electrical conductivity and a secondary Bi phase which are signs of the expected Mg-deficiency. We will refer to these samples as Mg-poor and Mg-rich Mg_3Bi_2 rather than by the stoichiometry extracted from the EDS analysis.

As can be seen in Figure 1, X-ray diffraction reveals a rather amorphous character of the two types of deposited films after deposition. However, when annealed at 200 – 300 °C the diffraction peaks corresponding to the expected hexagonal Mg_3Bi_2 phase are clearly visible.

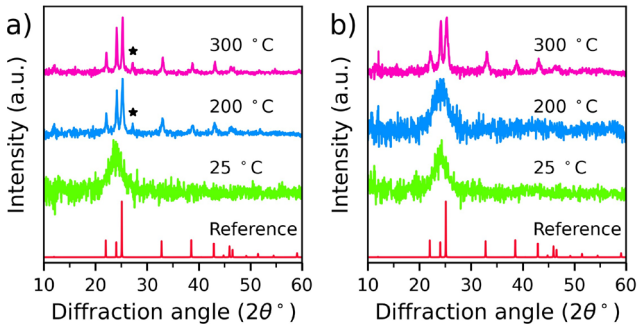

Figure 1. X-ray diffraction of (**a**) Mg-poor and (**b**) Mg-rich Mg_3Bi_2 thin films on room temperature substrates and after annealing at different temperatures. The red line corresponds to the ICSD pattern 659569 of Mg_3Bi_2. See Figures S2 and S3 as well as Table S1 for a more detailed XRD analysis.

Whole-pattern deconvolutions (Figures S2 and S3 and Table S1) reveal the crystallization of Mg_3Bi_2 in space group *P-3m1* with very similar lattice parameters (a=b=4.64 Å and c=7.37 Å for the Mg-poor sample and a=b=4.63 Å and c=7.37 Å for the Mg-rich one, both annealed at 300 °C), close to the reported values of a=b=4.67 Å and c=7.40 Å (ICSD reference 659569). In the case of the Mg-poor deposition, a clear signal for elemental bismuth is observed at 2θ=27.2° (see the diffraction peak with the star symbol in Figure 1a). This is consistent with a potential Mg-deficiency, as noted by others (we have taken this into account in the fit presented in Figure S2).[28,30] It is interesting to note that this bismuth phase vanishes when the Mg evaporation rate is increased (Figure 1b). The Mg-rich-deposited film requires a higher annealing temperature to crystallize than the Mg-poor film and remains less crystalline (broader diffraction peaks translating smaller crystallites) even at 300 °C.

Scanning electron microscopy images of both films can be found in Figure 2. They show small grains in all cases. The Mg-rich sample contains some domains of elevation due to the deposition, whereas the Mg-poor film is smooth. Elemental mapping (see Figure S4) of the Mg-rich film surface reveals that these domains are Mg-rich and could even represent elemental Mg clusters. Given that they are nanometric and relatively scarce on the surface their presence remains undetected by our

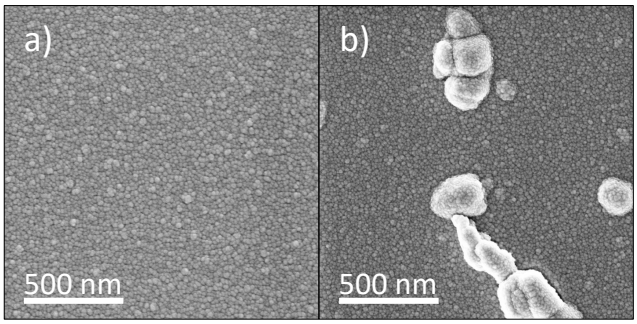

Figure 2. SEM images of (**a**) Mg-poor and (**b**) Mg-rich Mg_3Bi_2 taken at 50,000x magnification.

XRD equipment.

Given the successful deposition of Mg_3Bi_2 thin films with the correct crystalline phase, we investigated their thermoelectric properties from 30 to 200 °C. Figure 3a shows the relevant TE parameters (σ, S, κ, and ZT) obtained at different temperatures from the Mg-poor thin film. Before the measurement, the Mg-poor and Mg-rich Mg_3Bi_2 films were annealed at 200 °C for 1 hour.

The positive Seebeck and Hall coefficients indicate that the Mg-poor Mg_3Bi_2 thin film has a p-type conductivity, as expected from literature for Mg-deficient compositions.[11,12,17,34] The low thermal conductivity (κ) around 1 W/(m·K) at RT is comparable to other related Mg_3Bi_2-based compounds[14,22], although, to the best of our knowledge, an analogous value has not been reported so far for undoped Mg_3Bi_2. Regarding the electrical conductivity (σ), we find a value of ~80 × 10^3 S/m, which is higher than the electrical conductivity of Mg_3Bi_2 thin films deposited with magnetron sputtering.[28–30] The Seebeck coefficient across the selected temperature range has comparable values (40-60 µV/K) as found for the above-mentioned magnetron sputtered films and increases linearly with temperature. Such a linear increase of S with constant σ has also been observed in other inorganic semiconductor thin films.[6] This has been attributed to the shift of the Fermi level away from the valence band in heavily doped (degenerated) semiconductors or semimetals. [17,35]

Another key parameter which is often used to describe the quality of a thermoelectric material is the so-called power factor (PF):[36]

$$PF = \sigma \cdot S^2$$

We display the PF in Figure S5, with values ranging from 136 to 302 µW/(m·K^2) going from 30 to 200 °C. The PF of our Mg_3Bi_2 is superior to the typical values found in literature for Mg_3Bi_2.[28–30] The thermoelectric figure of merit ZT is around 0.04 at RT which increases to 0.11 at 200 °C. This is the first report of ZT values for undoped Mg_3Bi_2 thin films, as previous literature did not report on the thermal conductivity.

Furthermore, Hall effect measurements (Figure 3b) on the Mg-poor Mg_3Bi_2 thin film allow us to disentangle the charge carrier concentration (CCC) and mobility contributions to the electrical conductivity. Interestingly, these three parameters remain rather stable over the selected temperature range. The semi metallic behavior of Mg_3Bi_2 becomes apparent by the high carrier concentration of approximately 450 × 10^{18} cm^{-3}. It is important to note that the mobility is not affected by temperature, as one could expect from phonon scattering. Indeed, the hole mobility remains around 11 cm^2/(V·s) over the

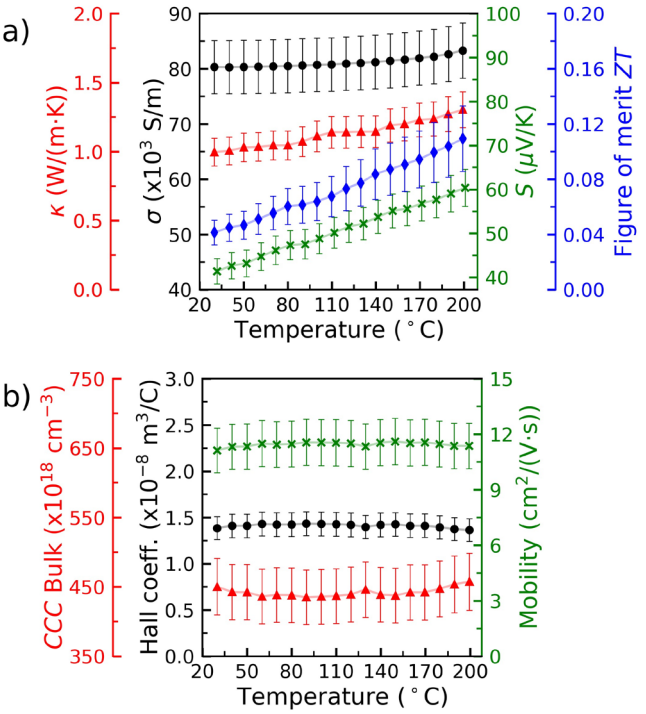

Figure 3. Temperature dependance of (**a**) the thermal conductivity (κ, red triangles), electrical conductivity (σ, black dots), Seebeck coefficient (S, green x's), thermoelectric figure of merit (ZT, blue diamonds), and (**b**) of the charge carrier concentration (CCC, red triangles), Hall coefficient (black dots), and hole mobility (green x's) of the Mg-poor Mg_3Bi_2 film. The error bars come from the deviation of the equipment.

temperature range from 30 to 200 °C.

When moving to films with a Mg-rich condition (Figure 4), the TE properties are changed drastically. For these films, the negative Seebeck coefficient is indicative of an n-type character which is in line with literature reports on bulk samples.[24,26] This highlights the versatility of thermal co-evaporation to tune the TE properties of Mg_3Bi_2 thin films. Moreover, despite a decrease in electrical conductivity with regards to the Mg-poor film, as the absolute Seebeck coefficient is increased and thermal conductivity becomes ultralow, the overall ZT is increased reaching 0.19 at 140 °C. It is important to note that, contrary to the Mg-poor sample, the electrical conductivity of the Mg-rich sample versus temperature is not monotonous, reaching a maximum around 140 °C – 170 °C. As σ is proportional to the product of the CCC and electron mobility. We can elucidate the trend of the conductivity by examining these two parameters in Figure 4b. The mobility has a maximum at 110 °C. In general, the charge mobility at lower temperatures is limited by impurity scattering, whereas at higher temperatures lattice scattering events become the dominant factor.[37,38] Further insights from theoretical calculations could assist in elucidating the exact scattering mechanisms at play and determining the density of state effective mass.[39] Since the CCC

gradually increases until a plateau is reached, σ reaches a maximum at a temperature slightly above that of the maximum mobility. Moreover, as the Seebeck coefficient is inversely proportional to the charge carrier concentration, it starts to decline as the *CCC* increases at 90 °C as can be seen in Figure 4a. Regarding the power factor (Figure S5) we observe a maximum of 193 μW/(m·K^2) around 130 °C which is lower than the Mg-poor analogue. The trend of the *PF* is mainly driven by the behavior of the electrical conductivity at higher temperature.

Hence, the thermoelectric properties of the Mg-rich Mg_3Bi_2 thin films are more complex than those of the Mg-poor Mg_3Bi_2 thin films caused primarily by a maximum in the charge carrier mobility. This is particularly the case in the temperature range of 80 – 110 °C (Figure 4). This can be attributed to competing impurity and lattice phonon scattering processes, dominant at lower and higher temperatures, respectively.[40,41] We should also remark that the measurements of the TE properties were conducted on Mg_3Bi_2 samples annealed at 200 °C, which is below the crystallization temperature (300 °C, see Figure 1b) of Mg-rich Mg_3Bi_2. Hence, the difference in TE performance could also be related to the difference in crystallinity between the Mg-poor and Mg-rich sample. This effect was demonstrated by others for GeSbTe thin films.[42] A follow-up study is required to elucidate how crystallinity affects the thermoelectric properties of Mg_3Bi_2 thin films.

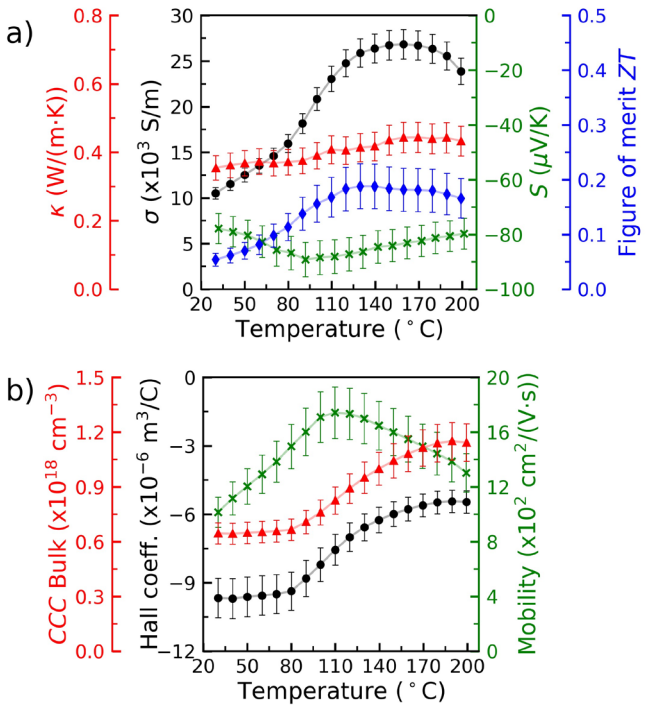

Figure 4. Temperature dependance of (**a**) the thermal conductivity (κ, red triangles), electrical conductivity (σ, black dots), Seebeck coefficient (S, green x's), thermoelectric figure of merit (ZT, blue diamonds), and (**b**) of the charge carrier concentration (*CCC*, red triangles), Hall coefficient (black dots), and hole mobility (green x's) of the Mg-rich Mg_3Bi_2 film. The error bars come from the deviation of the equipment.

In conclusion, we demonstrate that thermal vacuum co-deposition of Mg_3Bi_2 thin films enables the fine tuning of the stoichiometry. We determine the thermoelectric properties of two types of Mg_3Bi_2 thin films, one with a deficiency of Mg and one with an excess of Mg (the exact determination of thin films' stoichiometry in these cases remains a challenge that should be further investigated in future work). XRD analysis reveals the formation of the Mg_3Bi_2 phase in both cases upon annealing to 200 °C and 300 °C, respectively. The Mg-poor Mg_3Bi_2 films show a p-type behavior with a maximum ZT of 0.11 and a power factor of 302 μW/(m·K^2) at 200 °C. Through the incorporation of additional Mg during the thermal vacuum co-sublimation, a Mg-rich Mg_3Bi_2 film is obtained. The electrical behavior of these Mg-rich Mg_3Bi_2 thin films is changed from p- to n-type. The maximum ZT of 0.19 is obtained at 140 °C, and a power factor of 193 μW/(m·K^2) is observed at 130 °C. Due to the complex nature of the thermoelectric properties of the Mg-rich film, further studies into dominating carrier scattering mechanisms at different temperatures should be undertaken, possibly including theoretical calculations. We demonstrate that the stoichiometry of Mg_3Bi_2-based materials governs the nature of the electrical behavior, which can be tuned according to the deposition rate in a thermal co-deposition process. This can be utilized to fabricate thin film thermoelectric generators consisting of both p- and n-type Mg_3Bi_2 "legs".

Supporting Information

This material is available free of charge via the Internet at http://pubs.acs.org.

Detailed experimental procedures, EDS spectra, XRD fits, Le Bail fit results, SEM EDS images, and the power factor plot of Mg-poor and Mg-rich Mg_3Bi_2.

AUTHOR INFORMATION

Corresponding Authors

Francisco Palazon. Departamento de Ingeniería Química y Ambiental, Universidad Politécnica de Cartagena, 30202 Cartagena, Spain; https://orcid.org/0000-0002-1503-5965
Email: francisco.palazon@upct.es

Henk J. Bolink. Instituto de Ciencia Molecular, ICMol, Universidad de Valencia, 46980 Paterna, Spain;
https://orcid.org/0000-0001-9784-6253
Email: henk.bolink@uv.es

Cristina Roldán-Carmona. Instituto de Ciencia Molecular, ICMol, Universidad de Valencia, 46980 Paterna, Spain;
https://orcid.org/0000-0001-9624-3864
Email: cristina.roldan@uv.es

Authors

Joost W.C. Reinders. Instituto de Ciencia Molecular, ICMol, Universidad de Valencia, 46980 Paterna, Spain;
https://orcid.org/0009-0008-3618-256X

Author Contributions

The manuscript was written through contributions of all authors.

Notes

The authors declare no competing financial interest.

ACKNOWLEDGMENT

The authors gratefully acknowledge the financial support of the European Research Council (ERC) under the European Union's Horizon 2020 research and innovation program (Grant Agreement No. 834431), the Spanish Agencia Estatal de Investigaciones (AEI) project CEX2019-000919-M funded by MCIN/AEI/10.13039/501100011033 and project PID2021-

126444OB-I00 funded by MCIN/AEI/10.13039/501100011033 and by "ERDF A way of making Europe" as well as grants RYC2019-027187-I and RYC2020-028803-I funded by MCIN/AEI/10.13039/501100011033 and "ESF Investing in your future" and project TED2021-129609B-I00 funded by MCIN/AEI /10.13039/501100011033 and by European Union NextGenerationEU/ PRTR.

REFERENCES

(1) Snyder, J. G.; Toberer, E. S. Complex Thermoelectric Materials. *Nat Mater* **2008**, *7*, 105–114. https://doi.org/https://doi.org/10.1038/nmat2090.

(2) Massetti, M.; Jiao, F.; Ferguson, A. J.; Zhao, D.; Wijeratne, K.; Würger, A.; Blackburn, J. L.; Crispin, X.; Fabiano, S. Unconventional Thermoelectric Materials for Energy Harvesting and Sensing Applications. *Chem Rev* **2021**, *121* (20), 12465–12547. https://doi.org/10.1021/acs.chemrev.1c00218.

(3) Chen, X.; Dai, W.; Wu, T.; Luo, W.; Yang, J.; Jiang, W.; Wang, L. Thin Film Thermoelectric Materials: Classification, Characterization, and Potential for Wearable Applications. *Coatings* **2018**, *8* (7), 244. https://doi.org/10.3390/coatings8070244.

(4) Isotta, E.; Andrade-Arvizu, J.; Syafiq, U.; Jiménez-Arguijo, A.; Navarro-Güell, A.; Guc, M.; Saucedo, E.; Scardi, P. Towards Low Cost and Sustainable Thin Film Thermoelectric Devices Based on Quaternary Chalcogenides. *Adv Funct Mater* **2022**, *32*, 2202157. https://doi.org/10.1002/adfm.202202157.

(5) Sebastia-Luna, P.; Pokharel, U.; Huisman, B. A. H.; Koster, L. J. A.; Palazon, F.; Bolink, H. J. Vacuum-Deposited Cesium Tin Iodide Thin Films with Tunable Thermoelectric Properties. *ACS Appl Energy Mater* **2022**, *5* (8), 10216–10223. https://doi.org/10.1021/acsaem.2c01936.

(6) Liu, T.; Zhao, X.; Li, J.; Liu, Z.; Liscio, F.; Milita, S.; Schroeder, B. C.; Fenwick, O. Enhanced Control of Self-Doping in Halide Perovskites for Improved Thermoelectric Performance. *Nat Commun* **2019**, *10*, 5750. https://doi.org/10.1038/s41467-019-13773-3.

(7) Zhou, C.; Lee, Y. K.; Yu, Y.; Byun, S.; Luo, Z. Z.; Lee, H.; Ge, B.; Lee, Y. L.; Chen, X.; Lee, J. Y.; Cojocaru-Mirédin, O.; Chang, H.; Im, J.; Cho, S. P.; Wuttig, M.; Dravid, V. P.; Kanatzidis, M. G.; Chung, I. Polycrystalline SnSe with a Thermoelectric Figure of Merit Greater than the Single Crystal. *Nat Mater* **2021**, *20*, 1378–1384. https://doi.org/10.1038/s41563-021-01064-6.

(8) Zhang, Q.; Deng, K.; Wilkens, L.; Reith, H.; Nielsch, K. Micro-Thermoelectric Devices. *Nat Electron* **2022**, *5*, 333–347. https://doi.org/10.1038/s41928-022-00776-0.

(9) Ao, D. W.; Liu, W. Di; Zheng, Z. H.; Shi, X. L.; Wei, M.; Zhong, Y. M.; Li, M.; Liang, G. X.; Fan, P.; Chen, Z. G. Assembly-Free Fabrication of High-Performance Flexible Inorganic Thin-Film Thermoelectric Device Prepared by a Thermal Diffusion. *Adv Energy Mater* **2022**, *12* (42), 2202731. https://doi.org/10.1002/aenm.202202731.

(10) Wei, M.; Shi, X. L.; Zheng, Z. H.; Li, F.; Liu, W. Di; Xiang, L. P.; Xie, Y. S.; Chen, Y. X.; Duan, J. Y.; Ma, H. L.; Liang, G. X.; Zhang, X. H.; Fan, P.; Chen, Z. G. Directional Thermal Diffusion Realizing Inorganic Sb_2Te_3/Te Hybrid Thin Films with High Thermoelectric Performance and Flexibility. *Adv Funct Mater* **2022**, *32* (45), 2207903. https://doi.org/10.1002/adfm.202207903.

(11) Mao, J.; Zhu, H.; Ding, Z.; Liu, Z.; Gamage, G. A.; Chen, G.; Ren, Z. High Thermoelectric Cooling Performance of N-Type Mg_3Bi_2-Based Materials. *Science (1979)* **2019**, *365* (6452), 495–498. https://doi.org/10.1126/science.aax7792.

(12) Imasato, K.; Wood, M.; Anand, S.; Kuo, J. J.; Snyder, G. J. Understanding the High Thermoelectric Performance of Mg_3Sb_2-Mg_3Bi_2 Alloys. *Adv Energy Sustainability Res* **2022**, *3* (6), 2100208. https://doi.org/10.1002/aesr.202100208.

(13) Shang, H.; Liang, Z.; Xu, C.; Mao, J.; Gu, H.; Ding, F.; Ren, Z. N-Type $Mg_3Sb_{2-x}Bi_x$ Alloys as Promising Thermoelectric Materials. *Research* **2020**, *2020*, 1219461. https://doi.org/10.34133/2020/1219461.

(14) Imasato, K.; Kang, S. D.; Snyder, G. J. Exceptional Thermoelectric Performance in $Mg_3Sb_{0.6}Bi_{1.4}$ for Low-Grade Waste Heat Recovery. *Energy Environ Sci* **2019**, *12* (3), 965–971. https://doi.org/10.1039/c8ee03374a.

(15) Zhu, B.; Liu, X.; Wang, Q.; Qiu, Y.; Shu, Z.; Guo, Z.; Tong, Y.; Cui, J.; Gu, M.; He, J. Realizing Record High Performance in N-Type Bi_2Te_3-Based Thermoelectric Materials. *Energy Environ Sci* **2020**, *13* (7), 2106–2114. https://doi.org/10.1039/d0ee01349h.

(16) Witting, I. T.; Chasapis, T. C.; Ricci, F.; Peters, M.; Heinz, N. A.; Hautier, G.; Snyder, G. J. The Thermoelectric Properties of Bismuth Telluride. *Adv Electron Mater* **2019**, *5* (6), 1800904. https://doi.org/10.1002/aelm.201800904.

(17) Ponnambalam, V.; Morelli, D. T. On the Thermoelectric Properties of Zintl Compounds $Mg_3Bi_{2-x}Pn_x$ (Pn = P and Sb). *J Electron Mater* **2013**, *42* (7), 1307–1312. https://doi.org/10.1007/s11664-012-2417-7.

(18) Han, Z.; Gui, Z.; Zhu, Y. B.; Qin, P.; Zhang, B.-P.; Zhang, W.; Huang, L.; Liu, W. The Electronic Transport Channel Protection and Tuning in Real Space to Boost the Thermoelectric Performance of $Mg_{3+\delta}Sb_{2-y}Bi_y$ near Room Temperature. *Research* **2020**, *2020*, 1672051. https://doi.org/10.34133/2020/1672051.

(19) Shang, H.; Zhang, J.; Gu, H.; Song, S.; Chen, C. L.; Lee, J. F.; Shih, K.; Ren, Z.; Ding, F. Depressed Lattice Oxygen and Improved Thermoelectric Performance in

N-Type $Mg_3Bi_{2-x}Sb_x$ via La-Doping. *Mater Today Phys* **2021**, *21*, 100485. https://doi.org/10.1016/j.mtphys.2021.100485.

(20) Li, X.; Yang, B.; Xie, H.; Zhong, H.; Feng, S.; Zhang, Y.; Ma, Y.; Zhang, J.; Su, H. Synergistic Effects of Mg Vacancy and Ag Doping on Thermoelectric Transport Properties of P-Type Mg_3Sb_2. *Mater Res Bull* **2023**, *159*, 112106 2. https://doi.org/10.1016/j.materresbull.2022.112106.

(21) Chen, Y.; Li, L.; Li, S.; Yang, G.; Peng, P.; Wang, C. Enhanced Thermoelectric Performance of N-Type Mg_3Bi_2-Based Materials by Se Doping and Alloying Engineering. *J Phys D Appl Phys* **2022**, *55* (43), 434001. https://doi.org/10.1088/1361-6463/ac848e.

(22) Mo, X.; Liao, J.; Yuan, G.; Zhu, S.; Lei, X.; Huang, L.; Zhang, Q.; Wang, C.; Ren, Z. High Thermoelectric Performance at Room Temperature of N-Type Mg_3Bi_2-Based Materials by Se Doping. *J Magnesium Alloys* **2022**, *10* (4), 1024–1032. https://doi.org/10.1016/j.jma.2020.11.023.

(23) Zhang, J.; Song, L.; Borup, K. A.; Jørgensen, M. R. V.; Iversen, B. B. New Insight on Tuning Electrical Transport Properties via Chalcogen Doping in N-Type Mg_3Sb_2-Based Thermoelectric Materials. *Adv Energy Mater* **2018**, *8* (16), 1702776. https://doi.org/10.1002/aenm.201702776.

(24) Shuai, J.; Ge, B.; Mao, J.; Song, S.; Wang, Y.; Ren, Z. Significant Role of Mg Stoichiometry in Designing High Thermoelectric Performance for $Mg_3(Sb,Bi)_2$-Based n-Type Zintls. *J Am Chem Soc* **2018**, *140* (5), 1910–1915. https://doi.org/10.1021/jacs.7b12767.

(25) Imasato, K.; Ohno, S.; Kang, S. D.; Snyder, G. J. Improving the Thermoelectric Performance in $Mg_{3+x}Sb_{1.5}Bi_{0.49}Te_{0.01}$ by Reducing Excess Mg. *APL Mater* **2018**, *6* (1), 016106. https://doi.org/10.1063/1.5011379.

(26) Zhang, X.; Cao, X.; Zhang, Y.; Gu, H.; Liu, J.; Han, G.; Zhang, B.; Wang, G.; Zhou, X. Revealing the Intrinsic p-to-n Transition Mechanism on Mg_3Sb_2 through Extra Mg. *Appl Phys Lett* **2022**, *120* (17), 173902. https://doi.org/10.1063/5.0088156.

(27) Ying, P.; He, R.; Mao, J.; Zhang, Q.; Reith, H.; Sui, J.; Ren, Z.; Nielsch, K.; Schierning, G. Towards Tellurium-Free Thermoelectric Modules for Power Generation from Low-Grade Heat. *Nat Commun* **2021**, *12* (1), 1121. https://doi.org/10.1038/s41467-021-21391-1.

(28) Sadowski, G.; Zhu, Y.; Shu, R.; Feng, T.; Le Febvrier, A.; Music, D.; Liu, W.; Eklund, P. Epitaxial Growth and Thermoelectric Properties of Mg_3Bi_2 Thin Films Deposited by Magnetron Sputtering. *Appl Phys Lett* **2022**, *120* (5), 051901. https://doi.org/10.1063/5.0074419.

(29) Fang, W.; Zhu, W.; Shao, Y.; Zheng, P.; Si, J. Formation of Metastable Cubic Phase and Thermoelectric Properties in Mg_3Bi_2 Films Deposited by Magnetron Sputtering. *Appl Surf Sci* **2022**, *596*, 153602. https://doi.org/10.1016/j.apsusc.2022.153602.

(30) Tani, J. ichi; Ishikawa, H. Fabrication and Analysis of Mg_3Bi_2 Thin Films by Post Annealing Mg/Bi Bilayer Thin Films. *Mater Lett* **2023**, *331*, 133460. https://doi.org/10.1016/j.matlet.2022.133460.

(31) Long, A. R.; Macleod, A. M. A Co-Evaporation Control System for Two-Component Alloys. *J Phys E: Sci Instrum* **1979**, *12*, 205–211. https://doi.org/10.1088/0022-3735/12/3/016.

(32) Iwanaka, T.; Kusunoki, T.; Kotaki, H.; Kodama, M.; Tanaka, H.; Matsumoto, A.; Horii, S.; Doi, T. New Deposition Method of MgB_2 Thin Film with Thermal Evaporation of Mg and Sputtering of B. *Mater Res Express* **2020**, *7* (5), 056003. https://doi.org/10.1088/2053-1591/ab945a.

(33) Wang, H.; Ouyang, L. Z.; Zeng, M. Q.; Zhu, M. Hydrogen Sorption Properties of Mg/Mm-Ni Multi-Layer Film Prepared by Thermal Evaporation. *J Alloys Compd* **2004**, *375* (1–2), 313–317. https://doi.org/10.1016/j.jallcom.2003.12.009.

(34) Pan, Y.; Yao, M.; Hong, X.; Zhu, Y.; Zhu, Y.; Fan, F.; Imasato, K.; He, Y.; Hess, C.; Fink, J.; Fink, J.; Fink, J.; Yang, J.; Büchner, B.; Büchner, B.; Fu, C.; Snyder, G. J.; Felser, C. $Mg_3(Bi,Sb)_2$ Single Crystals towards High Thermoelectric Performance. *Energy Environ Sci* **2020**, *13* (6), 1717–1724. https://doi.org/10.1039/d0ee00838a.

(35) Shi, X.; Zhang, X.; Ganose, A.; Park, J.; Sun, C.; Chen, Z.; Lin, S.; Li, W.; Jain, A.; Pei, Y. Compromise between Band Structure and Phonon Scattering in Efficient N-$Mg_3Sb_{2-x}Bi_x$ Thermoelectrics. *Mater Today Phys* **2021**, *18*, 100362. https://doi.org/10.1016/j.mtphys.2021.100362.

(36) Zhao, L.-D.; Tan, G.; Hao, S.; He, J.; Pei, Y.; Chi, H.; Wang, H.; Gong, S.; Xu, H.; Dravid, V. P.; Uher, C.; Snyder, G. J.; Wolverton, C.; Kanatzidis, M. G. Ultrahigh Power Factor and Thermoelectric Performance in Hole-Doped Single-Crystal SnSe. *Science (1979)* **2015**, *351* (6269), 141–144. https://doi.org/10.1126/science.aad3749.

(37) Kuo, J. J.; Kang, S. D.; Imasato, K.; Tamaki, H.; Ohno, S.; Kanno, T.; Snyder, G. J. Grain Boundary Dominated Charge Transport in Mg_3Sb_2-Based Compounds. *Energy Environ Sci* **2018**, *11* (2), 429–434. https://doi.org/10.1039/c7ee03326e.

(38) Chen, X.; Zhu, J.; Qin, D.; Qu, N.; Xue, W.; Wang, Y.; Zhang, Q.; Cai, W.; Guo, F.; Sui, J. Excellent Thermoelectric Performance of Boron-Doped n-Type Mg_3Sb_2-Based Materials via the Manipulation of Grain Boundary Scattering and Control of Mg Content. *Sci China Mater* **2021**, *64* (7), 1761–1769. https://doi.org/10.1007/s40843-020-1559-4.

(39) De Boor, J.; Berche, A.; Jund, P. Density of States Effective Mass for P-Type Mg_2Si-Mg_2Sn Solid Solutions: Comparison between Experiments and First-Principles Calculations. *J Phys Chem C* **2020**, *124* (28), 14987–14996. https://doi.org/10.1021/acs.jpcc.0c03105.

(40) Altunöz, S.; Çelik, H.; Cankurtaran, M. Temperature and Electric Field Dependences of the Mobility of Electrons in Vertical Transport in GaAs/$Ga_{1-y}Al_yAs$ Barrier Structures Containing Quantum Wells. *Cent Eur J Phys* **2008**, *6* (3), 479–490. https://doi.org/10.2478/s11534-008-0067-4.

(41) Zhang, Y.; Singh, J. The Use of Kubo Formula to Examine Low Temperature Transport Limited by Interface Roughness and Phonons in Metal-Oxide-Semiconductor Field Effect Transistors. *J Appl Phys* **1999**, *85* (4), 2213–2220. https://doi.org/10.1063/1.369529.

(42) Vora-Ud, A.; Horprathum, M.; Eiamchai, P.; Muthitamongkol, P.; Chayasombat, B.; Thanachayanont, C.; Pankiew, A.; Klamchuen, A.; Naenkieng, D.; Plirdpring, T.; Harnwunggmoung, A.; Charoenphakdee, A.; Somkhunthot, W.; Seetawan, T. Thermoelectric Properties of C-$GeSb_{0.75}Te_{0.5}$ to h-$GeSbTe_{0.5}$ Thin Films through Annealing Treatment Effects. *J Alloys Compd* **2015**, *649*, 380–386. https://doi.org/10.1016/j.jallcom.2015.07.120.

Table of Contents Graphic